

## Automated 3D Mapping and Quantification of Haversian Architecture in Bone Tissue

Alejandro Morales Betancourt<sup>1</sup>, Sergio A. Montelongo<sup>1</sup>, Mark R. Appleford<sup>1</sup>, Teja Guda<sup>1</sup>

<sup>1</sup>Department of Biomedical Engineering, University of Texas at San Antonio. One UTSA Circle, San Antonio, TX, 78249.

[Alejandro.MoralesBetancourt@utsa.edu](mailto:Alejandro.MoralesBetancourt@utsa.edu)

### Abstract

Bone tissue has a unique architecture necessitating laborious characterization at various scales. Since the extracellular matrix (ECM) exists in a solid phase, traditional histology reduces the mineral content of ECM to obtain high-resolution 3d micrographs and is operator dependent in terms of analysis. Other imaging techniques such as microCT ( $\mu$ CT), are limited by the spatial resolution of the  $\mu$ CT scanner and provide minimal cellular correlation. The vascularization inside the bone (Haversian system) appears to exist in continually remodeling patterns with bone turnover, making it difficult to numerically assess the Haversian canal architecture. Our novel technique proposes the 3D characterization of bone tissue, by using light microscopy and MATLAB®, to acquire microscopic 3D images of bone vasculature with enhanced spatial resolution. Briefly, the right femurs of eight rats were sectioned in cross sectional slices of 1 mm thickness. The slices were exposed to a Villanueva osteochrome stain protocol followed by sequential dehydration, poly methyl-methacrylate infiltration, and polymerization. Using a combination of a novel, automated focus-adjusting system in conjunction with light microscopy, we obtained 100 sequential discrete images at 1 $\mu$ m steps along the z-stack at 100x in-plane magnification. The images were processed using MATLAB® software, obtaining a 3D representation of the Haversian system. From these 3D images we quantified Haversian number, and vessel parameters, including surface, volume, channel thickness and porosity ratio to tissue volume. Data analysis shows differences in the Haversian thickness in the three regions studied, showing that the overall vessel volume remains relatively conserved, but the Haversian architecture changes further away from the proximal region. Due to optical microscope limitations, this technique only can measure samples up to 100 microns in depth. This protocol can potentially be used to obtain 3D architectural quantification of other tissues by modifying staining protocols.

**Keywords:** Haversian, three-dimensional, cortical bone.

## 1. Introduction

The microstructure of the compact bone is transient, governed by bone remodeling and modified by aging and pathologic conditions. Understanding the pore microstructure of compact bone such as the Haversian system allows the recognition of remodeling activity trends, distribution, and the pathogenesis of the osteoporosis, and other mechanisms, including homeostasis following a nonunion fracture healing process [1].

Due to the continuous remodeling of bone tissue, it is hard to reproduce a map that represents Haversian configurational trends, even within the same species. Previous studies showed a correlation of age and an increment in Haversian canal area as a proportion of total cross section bone area, and cortical bone area[2]. Differences among endosteal and periosteal Haversian distribution have been reported [1], in addition to the finding that the size of Haversian canals remains the same while the size of osteons themselves decreases with age[3]. Cortical resorption loci represent large cavities within the Haversian canals that are in juxtaposition of necrotic tissue regions[4]. These resorption centers become new Haversian formations to replace cortical bone tissue. In order to obtain a truthful characterization, it is necessary to consider bone tissue as a three-dimensional entity. Morphologic and morphometric studies of Haversian systems however is affected by user bias and artifacts inherent in characterization techniques[5].

While the architecture of trabecular networks in bone, especially using histomorphometry is well characterized, and standardized[6], the field of evaluating cortical bone porosity and quantifying it is an area of active development. Cooper et al.[7], noted that cortical porosity is a critical metric in determining the mechanical properties of cortical bone and serves as a predictor of local fracture risk. The cortical porosity is comprised of two distinct components: the Haversian network and the Lacunae-canalicular network (LCN). The Haversian canals, typically  $\sim 30\mu\text{m}$  in diameter, house the bone tissue vasculature which connects to the body's blood supply and are turned-over during bone remodeling. The LCN houses osteocytes, which are the bone cells (osteoblasts) that are trapped in the mineralized extracellular matrix deposited and form a connected distributed network throughout the bone matrix. The LCN pores are on the order of  $2\mu\text{m}$  in size and it is hypothesized that fluid flow in this network around the osteocytes is used to regulate bone tissue mechanical adaptation and homeostasis[8].

The size of the Haversian channels is at the cutting edge of the measurement resolution for in vivo CT scanners, while synchrotron sources are required for the measurement of LCN porosity[7, 9]. Cordoso et al.[8] thoroughly reviewed the techniques available to characterize the vascular and LCN porosity fractions in cortical bone and note that the techniques available to map the Haversian system architecture include: video microscopy (resolution  $\sim 20\mu\text{m}$ ), micro radiography (resolution  $\sim 5\mu\text{m}$ ), micro computed tomography ( $\mu\text{CT}$ , resolution  $\sim 1\mu\text{m}$ ), light microscopy ( resolution  $\sim 300\text{ nm}$ ) and confocal laser scanning microscopy (CLSM, resolution  $\sim 200\text{ nm}$ ). While CLSM has excellent multi-plane focus, it requires pre-staining with fluorescent tags and light microscopy has largely been limited to 2D analysis.

Literature reports suggest that not just local mineral density (usually obtained by radiographic techniques), but also local pore microarchitecture and microporosity play a crucial

role in determining the microstrains and hence the local mechanics of cortical bone tissue[10]. Hence, there is a need for a technique that is able to tie together the cellular tissue composition with a quantifiable three-dimensional analysis of cortical pore architecture. In the current study, we propose to develop a technique to automate pseudo-3D analysis of cortical bone micro-porosity, not by serial sections, but to leverage the thickness of a single histological section and an automated light microscopy platform to provide a less laborious alternative to confocal microscopy. We propose to validate our method by investigating the differences in Haversian canal distribution among anatomical locations at the distal, medial and proximal aspects of rat femoral cortices.

## **2. Materials and Methods**

### ***2.1 Sample Collection***

The right femurs of 8 healthy Sprague Dawley rats of 12 months of age were harvested and fixed in formaldehyde 4% for 1 week under vacuum to promote perfusion of the Haversian canals. The formaldehyde was refreshed every 48 hours to ensure fixation. The samples were then sectioned at 7, 14 and 21mm from the condyle, by using an IsoMet® 1000 Precision Saw (Buehler, Lake Bluff, IL) using a 0.264 mm diamond blade, to obtain three cross sections per sample of 1mm thickness each; at the designated proximal, medial and distal anatomical locations.

### ***2.2 Histology***

The sections were placed in 10 ml capped glass bottles containing 3 ml of Villanueva Osteochrome, and placed under agitation for 7 days. Serial dehydration was performed in each sample, by changing the samples to a clean 10 ml glass capped bottles, with the following dilutions:

- a. 6 ml of 70% Ethanol: 30% Distilled Water, for 90 minutes.
- b. 6 ml of 90% Ethanol: 10% Distilled Water, for 17 hours.
- c. 6 ml of 100% Ethanol, for 180 minutes.

Plastic infiltration was performed for each sample, via Xylene-ethanol exchange followed by successive polymer-xylene exchange to match solvents. This was conducted by changing the samples to a clean 10 ml glass capped bottles, with the following dilutions:

- d. 6 ml 90 % Xylenes: 10% Ethanol, for 150 minutes.
- e. 6 ml of 100% Xylenes, for 150 minutes.
- f. 6 ml of 70% Technovit® 7200: 30% Xylenes, 48 hours.
- g. 6 ml of 90% Technovit® 7200: 10% Xylenes, for 17 hours.
- h. 6 ml of 100% Technovit® 7200, for 1 day.
- i. 6 ml of 100% Technovit® 7200, for 8 days.

The samples were then transferred to a peel-off plastic container with 6 ml of fresh Technovit® 7200 and placed under white light for polymerization during 10 hours. Samples were ground down using a Struer LaboPol-5 grinder and glued with Technovit® 4000 to an EXAKT P/N 41502 back slide. The back slide was attached to an EXAKT 400 CS micro-grinding system (Nordestedt, Germany) and the polymer blocks were shaved down to expose the sample; then, glued with Technovit® 9100 to an EXACT P/N 41500 final slide, and place under UV light for 15 minutes. The final slides were attached to an EXAKT 300 CL system to cut the back slide portion from the block. The final slide was placed into an EXAKT 400 CS micro grinding system and shaved down to 1 mm thickness with 800 grit sandpaper. The sample was then further polished within the same device by using 4000 grit sandpaper.

### ***2.3 Data acquisition and image reconstruction***

The final slide was observed under a Leica DMI LED Light Microscope at 100X magnification. Two region of interest were selected in opposite sides of the bone sample. The microscope was attached to a computer running the Bioquant Osteo program, and to a QImage camera system. The threshold of the program was keep constant for every sample at R:35,15; G:26,10; B:19,9. A custom macro was written to automate the measurements of the Bioquant Osteo program, and programed to make 100 measurements per sample. This step saved an estimated 500 hours of man power dedicated to manually selecting the threshold and performing the measurements for the sample. A motor commanded by a microcontroller using an Arduino<sup>®</sup> board, was synchronized with the macro that ran Bioquant Osteo to change the focus of the microscope by 1  $\mu\text{m}$  between measurements, which improved process accuracy and repeatability by eliminating user induced error. Raw data was organized using a customized Matlab<sup>®</sup> script to transform data points to three dimensional planes corresponding to each of the one hundred planes measured for each sample to create an image stack. The planes then were reconstructed using ImageJ software (NIH) to obtain a three-dimensional image of the Haversian canals.

### ***2.4 Data and Statistical Analysis***

The 3D reconstructions were then analyzed by using CTAn program (Bruker) to obtain Haversian volume, haversian volume/tissue volume fraction, haversian surface, haversian surface density, haversian connectivity, haversian pattern factor, haversian spacing and haversian channel thickness. Statistical analysis was performed using SigmaPlot 13.0 (Systat, San Jose, CA) to evaluate parametric differences between anatomical locations proximal, middle and distal as the primary variable. If the Shapiro-Wilk test for normality or the Brown Forsythe test for equal variance between groups was not satisfied, then the Kruskal Wallis ANOVA on ranks was run as a non-parametric test. If any significant differences between groups was identified, multiple comparisons were conducted to identify differences using Dunn's test and correction for multiple comparisons (significance determined at  $p < 0.05$ ). The normality test failed for the Haversian volume, Haversian surface, Haversian channel thickness, Haversian connectivity and Haversian spacing measures; while the equal variance test failed for the Haversian pattern factor. When the data was normally distributed and had equal variance (Haversian surface density), one way ANOVA was conducted, followed by pairwise differences being compared post hoc using the Holm-Sidak test and corrected for multiple comparisons (significance determined at  $p < 0.05$ ).

## **3. Results**

The reconstruction of the raw data provide us a three-dimensional map of 600 x 400 x 100  $\mu\text{m}^3$  volume of each sample with a nominal voxel side resolution of 1  $\mu\text{m}$  (**Figure 1**). In the histological image details of the lacunae-canalicular system, and in the reconstructed image, the extracted Haversian canals architecture could be observed. Representative images show the variations with anatomical location in the proximal, middle and distal femur of the Haversian channel network prior to morphometric quantification (**Figure 2**).

## Automated 3D Mapping of Haversian System

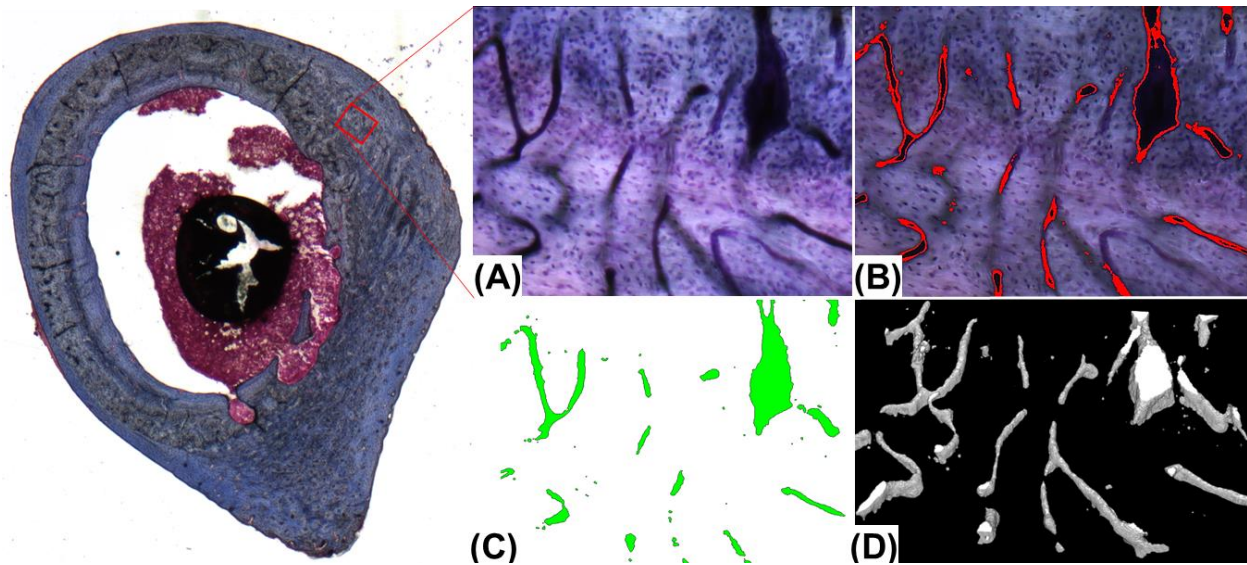


**Figure 1. Reconstruction of a Distal Section of the Rat Femur.** Data acquisition progression, beginning from the (left panel) histological cross section of the rat femur, counterstained to enhance the haversian systems in bone, followed by (A) Light microscopy imaging at high magnification, (B) color thresholding based region of interest identification (red boundary detection), (C) plane creation based on data acquisition and import into a digital binarized matrix format using Matlab®, and (D) the three-dimensional reconstruction of one hundred individual planes of raw data using ImageJ™ to obtain a 600 x 400 x 100  $\mu\text{m}^3$  volume of interest for further quantification.



**Figure 2. Variations in the pore architecture along the length of the Rat Femur.** Representative 3D rendering of the Haversian porous architecture at the (A) Proximal, (B) Middle and (C) Distal aspect of the rat femur within the cortical bone, represents clear variations in the extent and distribution of porosity. The variations and changes in such porosity if quantified can be correlated to maintenance of bone physiology or turnover and potentially used as predictors of pathological conditions.

The primary metrics of cortical porosity were not found to be different between the three anatomical locations. Neither absolute Haversian volume nor cortical bone pore fraction ( $p=0.073$  and  $p=0.076$  respectively between proximal and middle sections) indicated any significant difference based on anatomical location (**Figure 3**). The architectural parameters though indicated significant differences across surface area (**Figure 4 A,D**), channel connectivity (**Figure 4 B,E**) and channel morphology (**Figure 4 C,F**). Significantly greater Haversian surface area was observed in the distal sections compared to the middle ( $p=0.005$ ), with the Haversian surface density being significantly greater in the distal aspect compared to both the proximal and middle sections ( $p<0.001$ ). The Haversian connectivity indicated that the channels were least branched in the middle section ( $p<0.05$ ), which matches the estimate of organized longitudinal Haversian systems in the diaphysis while the Haversian pattern factor was significantly lower

(indicating convergent pore structures) in the proximal section compared to distal ( $p=0.003$ ). Distal sections showed the smallest channel thickness ( $p=0.041$  compared to proximal) and inter-channel spacing ( $p=0.005$  compared to middle).

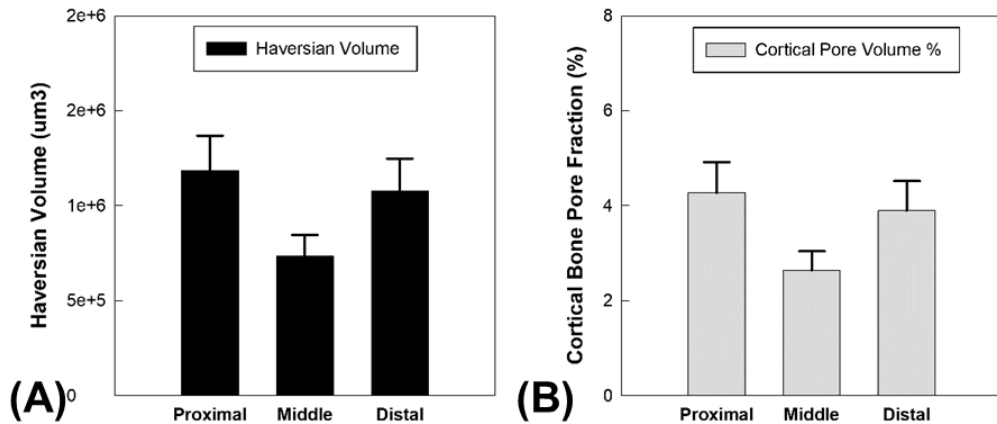


**Figure 3. Quantification of the Cortical Porosity within Bone Tissue.** No significant differences were observed within the cortical porosity measured at the proximal, middle and distal locations in terms of the (A) Haversian pore volume or the (B) porosity fraction of the cortices.

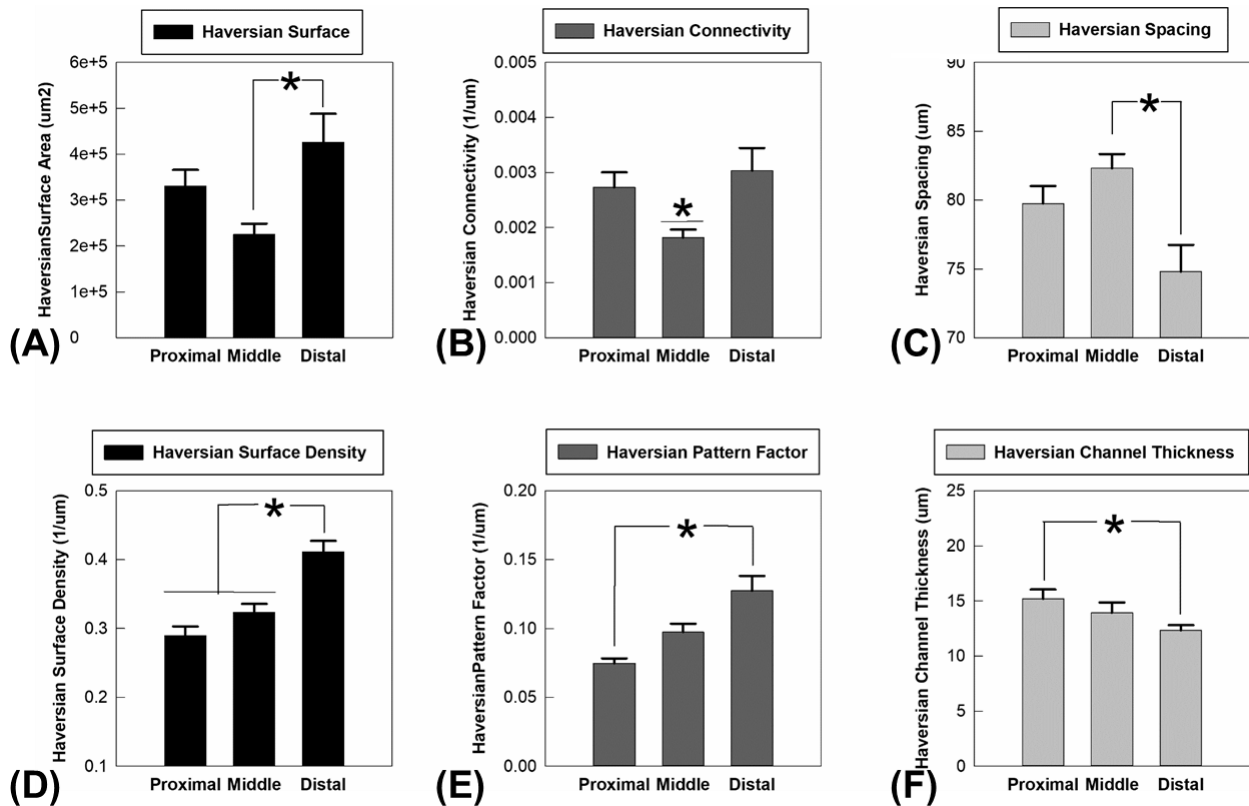


**Figure 4. Haversian Architecture and Pattern Quantification within Bone Tissue.** Differences in pore surface area indicated by (A) Haversian Surface and (D) Haversian Surface Density; channel connectivity represented by (B) Haversian Connectivity and (E) Haversian Pattern Factor and channel morphology quantified as (C) Haversian Spacing and (F) Haversian Channel Thickness showed significant pore architecture variations between the proximal, middle and distal sections (\* indicates significant differences at  $p<0.05$ ).

#### 4. Discussion and Conclusions

Variations in cortical bone porosity are of great interest from a research standpoint not only because of predictive bone fracture risk, but also because they have been found to correlate to hormone levels (such as parathyroid hormone) and age[11], as well as indicate the clinical efficacy of therapies against pathologies such as osteoporosis[12]. The use of characterization techniques such as acoustic impedance microscopy enables the acquisition of material property as well as porosity data in clinical settings, but is limited in terms of detecting tissue and cellular effects[13]. Synchrotron based micro computed tomography has been the most sensitive to detecting changes in bone microporosity[13], and has become the method of choice[14]. Due to the extent of the artifacts involved in acquisition, sensitivity to x-ray flux and the dose of radiation involved, quantitative synchrotron  $\mu$ CT remains an ex vivo technique[15]. Additionally, in a detailed review of available CT techniques, Peyrin et al[15] note that while synchrotron  $\mu$ CT is adept at detecting pore architecture, including at the LCN level, it only detects the pore spaces, not necessarily identifying whether those spaces are occupied by osteocytes. Automated network quantification of the data acquired by such techniques is also fairly limited[15] and not extensively standardized. Alternative techniques available for mapping cortical porosity, such as the LCN, include the focused ion beam (FIB) based milling combined with scanning electron microscopy (SEM)[16]; or synchrotron phase contrast based nanoCT[17], both of which are essentially destructive/ex vivo methods that are used on bone biopsy cores for LCN quantification. In terms of the cortical porosity measurement, the use of nuclear magnetic resonance (NMR) imaging has also been reported[18], but such use has been limited due to resource availability.

The cortical porosity at the osteocyte level has been extensively investigated, based on the hypothesis that the LCN network and fluid flow within influence the regulation of bone matrix production and resorption as well as calcium homeostasis; releases fibroblast growth factor 23 to regulate phosphate homeostasis; and potentially also has endocrine functions[19]. The fluid flow within the LCN itself is load induced, but is architecture dependent[20]. Alterations in LCN have been linked to estrogen deficiency indicating its value as a pathological marker[21]; and it has been demonstrated that LCN architecture varies greatly with bone compartment, age and disease[22], which further supports the value of quantifying the LCN. In an attempt to validate the hypothesis that the osteocyte morphologies and their organization in the LCN are what underlies bone tissue mechano-sensing[23], Kerschnitzki et al.[24] used rhodamine dye in conjunction with histology and laser scanning confocal microscopy to skeletonize the osteocyte network and compute linkages. While histology remains the gold standard for the quantification of cortical porosity, serial histological sections followed by stereology (and even fluorescent dye tagging) is an extremely labor intensive process[16].

The method demonstrated within this study overcomes the limitations of 2D histology, works from a single histological section and identifies the Haversian network across a 100  $\mu$ m depth at a detailed in-plane resolution using light microscopy. The user-independent measurement reduces bias and the quantification of the cortical porosity now forms a bridge between fully quantifiable modalities such as  $\mu$ CT and biological and cellular quality measurement that histology provides. The value of quantifying cortical porosity at the Haversian level is of tremendous value, as demonstrated by the studies of Malo et al.[25], who showed that longitudinal bone porosity varies with age and reported cortical porosity fractions ranging between 7 and 13.5% and Bousson et al.[26], who studied porosity in the femoral neck of women with an average age of 87 years, but without osteoporosis and found a cortical porosity range of 5-39%, with an average of 16%. Three

dimensional synchrotron  $\mu$ CT[27] has reported a cortical porosity of 10% in long bones, while a similar value was reported in human mandibles ( $10 \pm 9\%$ ) using two dimensional histomorphometrics[28]. This metric has been referred to as “canal volume fraction” to indicate that the Haversian and Volkmann’s canals (which are Haversian canal interconnections) were quantified[27]. In addition to cortical porosity, the size of the cortical pores has also been quantified using sphere filling algorithms often used in three dimensional  $\mu$ CT quantification to indicate pore and channel sizes ranging between 50 and 850  $\mu$ m in the appendicular skeleton [29]. There have been concerns with the correlation between histological and  $\mu$ CT measurements though, because Recker et al.[30] report a clinical trial in which cortical porosity was found to change significantly and was numerically greater when measured by  $\mu$ CT, but was not supported by histomorphometry. This is potentially because of a 2D metric being compared to a 3D metric head-to-head. Our proposed method overcomes these limitations by using identical algorithms for calculating quantitative architectural metrics from histology, using programs used currently for tomographic analysis. This continues the work of Cooper et al.[31] who attempted to normalize the cortical porosity architectural metrics to the systematic nomenclature proposed by Parfitt and colleagues[6] for all bone histomorphometry.

Within the design of the current study, which attempted to evaluate a novel technique to distinguish the baseline variations in cortical bone Haversian porosity and its architecture in the femoral cortices of skeletally mature rats; as separated by bone compartment, we found that our technique was reproducible and statistically sensitive within the sample size chosen. Data analysis shows some differences in the Haversian structure based on the anatomical location of the vasculature, in general the vessel volume was conserved along the femur, but the thickness of the vessel was significantly smaller as the measurement was getting farther away from the proximal region. Limitations of the study include the fact that rodents are known to have a lamellar bone structure with true Haversian systems only developing with skeletal aging[32]. While all the animals in our study were skeletally mature are determined by stabilization of body mass, they were not gender controlled and as such, the results of the current study should only be extrapolated across age-matched controls. Additionally, statistical power could potentially be increased by pairing samples within the same animal, but within the limitations of the study this was not deemed appropriate since regions within the animal were chosen at random and effects of periosteal and endosteal bias as well as radial bias are well documented.

In conclusion we found that automating sequential stereographic acquisition, color based thresholding and stereography based three-dimensional morphometric analysis when paired together were sensitive to detecting changes in the Haversian porosity within cortical bones of rats. When bone compartment and anatomical location, age and gender variations are accounted for, this novel technique provides a relatively low-resource correlation of tissue histological data to true radiographic computed tomography quantification of architecture.

### 5. Acknowledgments

AMB was supported in part by the National Science Foundation Louis Stokes Alliances for Minority Participation grant (Award No. 1305001) and the National Institutes of Health/NIGMS MARC U\*STAR (#GM07717-37) and RISE (#GM60655-16) awards. TG and SAM were supported in part by a sub-award of the National Institutes of Health (R21DE022925). TG was further supported through US Army Medical Research (W81XWH-15-P-0214), StemBioSys Inc. and the UTSA Office of the Vice President of Research (GREAT mechanism).

## References

- [1] J.N. Kim, J.Y. Lee, K.J. Shin, Y.C. Gil, K.S. Koh, W.C. Song, Haversian system of compact bone and comparison between endosteal and periosteal sides using three-dimensional reconstruction in rat, *Anatomy & cell biology* 48(4) (2015) 258-61.
- [2] J. Black, R. Mattson, E. Korostoff, Haversian osteons: size, distribution, internal structure, and orientation, *Journal of biomedical materials research* 8(5) (1974) 299-319.
- [3] J. Jowsey, Studies of Haversian systems in man and some animals, *Journal of anatomy* 100(Pt 4) (1966) 857-64.
- [4] D.H. Enlow, Functions of the Haversian system, *The American journal of anatomy* 110 (1962) 269-305.
- [5] U.E. Pazzaglia, T. Congiu, M. Marchese, F. Spagnuolo, D. Quacci, Morphometry and patterns of lamellar bone in human Haversian systems, *Anatomical record* 295(9) (2012) 1421-9.
- [6] A.M. Parfitt, M.K. Drezner, F.H. Glorieux, J.A. Kanis, H. Malluche, P.J. Meunier, S.M. Ott, R.R. Recker, Bone histomorphometry: standardization of nomenclature, symbols, and units: report of the ASBMR Histomorphometry Nomenclature Committee, *Journal of bone and mineral research* 2(6) (1987) 595-610.
- [7] D.M.L. Cooper, J.R. Matyas, M.A. Katzenberg, B. Hallgrímsson, Comparison of Microcomputed Tomographic and Microradiographic Measurements of Cortical Bone Porosity, *Calcified Tissue International* 74(5) (2004) 437-447.
- [8] L. Cardoso, S.P. Fritton, G. Gailani, M. Benalla, S.C. Cowin, Advances in assessment of bone porosity, permeability and interstitial fluid flow, *Journal of Biomechanics* 46(2) (2013) 253-265.
- [9] D.M.L. Cooper, C.E. Kawalilak, K. Harrison, B.D. Johnston, J.D. Johnston, Cortical Bone Porosity: What Is It, Why Is It Important, and How Can We Detect It?, *Current Osteoporosis Reports* 14(5) (2016) 187-198.
- [10] T. Hoc, L. Henry, M. Verdier, D. Aubry, L. Sedel, A. Meunier, Effect of microstructure on the mechanical properties of Haversian cortical bone, *Bone* 38(4) (2006) 466-474.
- [11] R.M.D. Zebaze, A. Ghasem-Zadeh, A. Bohte, S. Iuliano-Burns, M. Mirams, R.I. Price, E.J. Mackie, E. Seeman, Intracortical remodelling and porosity in the distal radius and post-mortem femurs of women: a cross-sectional study, *The Lancet* 375(9727) (2010) 1729-1736.
- [12] J.R. Zanchetta, C.E. Bogado, J.L. Ferretti, O. Wang, M.G. Wilson, M. Sato, G.A. Gaich, G.P. Dalsky, S.L. Myers, Effects of Teriparatide [Recombinant Human Parathyroid Hormone (1–34)] on Cortical Bone in Postmenopausal Women With Osteoporosis, *Journal of Bone and Mineral Research* 18(3) (2003) 539-543.
- [13] D. Rohrbach, S. Lakshmanan, F. Peyrin, M. Langer, A. Gerisch, Q. Grimal, P. Laugier, K. Raum, Spatial distribution of tissue level properties in a human femoral cortical bone, *Journal of Biomechanics* 45(13) (2012) 2264-2270.
- [14] A. Pacureanu, M. Langer, E. Boller, P. Tafforeau, F. Peyrin, Nanoscale imaging of the bone cell network with synchrotron X-ray tomography: optimization of acquisition setup, *Medical Physics* 39(4) (2012) 2229-2238.
- [15] F. Peyrin, P. Dong, A. Pacureanu, M. Langer, Micro- and Nano-CT for the Study of Bone Ultrastructure, *Current Osteoporosis Reports* 12(4) (2014) 465-474.
- [16] P. Schneider, M. Meier, R. Wepf, R. Müller, Towards quantitative 3D imaging of the osteocyte lacuno-canalicular network, *Bone* 47(5) (2010) 848-858.
- [17] B. Hesse, P. Varga, M. Langer, A. Pacureanu, S. Schrof, N. Männicke, H. Suhonen, P. Maurer, P. Cloetens, F. Peyrin, K. Raum, Canalicular Network Morphology Is the Major Determinant of the Spatial Distribution of Mass Density in Human Bone Tissue: Evidence by Means of Synchrotron Radiation Phase-Contrast nano-CT, *Journal of Bone and Mineral Research* 30(2) (2015) 346-356.

- [18] X. Wang, Q. Ni, Determination of cortical bone porosity and pore size distribution using a low field pulsed NMR approach, *Journal of Orthopaedic Research* 21(2) (2003) 312-319.
- [19] P.R. Buenzli, N.A. Sims, Quantifying the osteocyte network in the human skeleton, *Bone* 75(Supplement C) (2015) 144-150.
- [20] C. Price, X. Zhou, W. Li, L. Wang, Real-time measurement of solute transport within the lacunar-canalicular system of mechanically loaded bone: Direct evidence for load-induced fluid flow, *Journal of Bone and Mineral Research* 26(2) (2011) 277-285.
- [21] D. Sharma, C. Ciani, P.A.R. Marin, J.D. Levy, S.B. Doty, S.P. Fritton, Alterations in the osteocyte lacunar–canalicular microenvironment due to estrogen deficiency, *Bone* 51(3) (2012) 488-497.
- [22] X. Lai, C. Price, S. Modla, W.R. Thompson, J. Caplan, C.B. Kirn-Safran, L. Wang, The dependences of osteocyte network on bone compartment, age, and disease, *Bone Research* 3 (2015) 15009.
- [23] R.P. van Hove, P.A. Nolte, A. Vatsa, C.M. Semeins, P.L. Salmon, T.H. Smit, J. Klein-Nulend, Osteocyte morphology in human tibiae of different bone pathologies with different bone mineral density — Is there a role for mechanosensing?, *Bone* 45(2) (2009) 321-329.
- [24] M. Kerschnitzki, P. Kollmannsberger, M. Burghammer, G.N. Duda, R. Weinkamer, W. Wagermaier, P. Fratzl, Architecture of the osteocyte network correlates with bone material quality, *Journal of Bone and Mineral Research* 28(8) (2013) 1837-1845.
- [25] M.K.H. Malo, D. Rohrbach, H. Isaksson, J. Töyräs, J.S. Jurvelin, I.S. Tamminen, H. Kröger, K. Raum, Longitudinal elastic properties and porosity of cortical bone tissue vary with age in human proximal femur, *Bone* 53(2) (2013) 451-458.
- [26] V. Bousson, F. Peyrin, C. Bergot, M. Hausard, A. Sautet, J.-D. Laredo, Cortical Bone in the Human Femoral Neck: Three-Dimensional Appearance and Porosity Using Synchrotron Radiation, *Journal of Bone and Mineral Research* 19(5) (2004) 794-801.
- [27] P. Dong, S. Hauptert, B. Hesse, M. Langer, P.-J. Gouttenoire, V. Bousson, F. Peyrin, 3D osteocyte lacunar morphometric properties and distributions in human femoral cortical bone using synchrotron radiation micro-CT images, *Bone* 60(Supplement C) (2014) 172-185.
- [28] Z. Tonar, I. Khadang, P. Fiala, L. Nedorost, P. Kochová, Quantification of compact bone microporosities in the basal and alveolar portions of the human mandible using osteocyte lacunar density and area fraction of vascular canals, *Annals of Anatomy - Anatomischer Anzeiger* 193(3) (2011) 211-219.
- [29] B.L. Jorgenson, H.R. Buie, D.D. McErlain, C. Sandino, S.K. Boyd, A comparison of methods for in vivo assessment of cortical porosity in the human appendicular skeleton, *Bone* 73(Supplement C) (2015) 167-175.
- [30] R.R. Recker, S.P. Bare, S.Y. Smith, A. Varela, M.A. Miller, S.A. Morris, J. Fox, Cancellous and cortical bone architecture and turnover at the iliac crest of postmenopausal osteoporotic women treated with parathyroid hormone 1–84, *Bone* 44(1) (2009) 113-119.
- [31] D.M.L. Cooper, A.L. Turinsky, C.W. Sensen, B. Hallgrímsson, Quantitative 3D analysis of the canal network in cortical bone by micro-computed tomography, *The Anatomical Record Part B: The New Anatomist* 274B(1) (2003) 169-179.
- [32] S.M. Tommasini, A. Trinward, A.S. Acerbo, F. De Carlo, L.M. Miller, S. Judex, Changes in intracortical microporosities induced by pharmaceutical treatment of osteoporosis as detected by high resolution micro-CT, *Bone* 50(3) (2012) 596-604.